RL-TR-97-45
Final Technical Report
July 1997

SUB-MILLIMETER WAVEGUIDE FOR MONOLITHIC CIRCUITS

University of Michigan

Nihad I. Dib and Linda P.B. Katehi

APPROVED FOR PUBLIC RELEASE; DISTRIBUTION UNLIMITED.

19970929 017

Rome Laboratory
Air Force Materiel Command
Rome, New York

This report has been reviewed by the Rome Laboratory Public Affairs Office (PA) and is releasable to the National Technical Information Service (NTIS). At NTIS it will be releasable to the general public, including foreign nations.

RL-TR-97-45 has been reviewed and is approved for publication.

APPROVED: *Andrew J. Slobodnik, Jr.*

ANDREW J. SLOBODNIK, JR.
Project Engineer

FOR THE COMMANDER:

HORST R. WITTMAN, Director
Electromagnetics & Reliability Directorate

If your address has changed or if you wish to be removed from the Rome Laboratory mailing list, or if the addressee is no longer employed by your organization, please notify RL/ERAC, 31 Grenier Street, Hanscom AFB MA 01731-3010. This will assist us in maintaining a current mailing list.

Do not return copies of this report unless contractual obligations or notices on a specific document require that it be returned.

REPORT DOCUMENTATION PAGE

Public reporting burden for this collection of information is estimated to average 1 hour per response, including the time for reviewing instructions, searching existing data sources, gathering and maintaining the data needed, and completing and reviewing the collection of information. Send comments regarding this burden estimate or any other aspect of this collection of information, including suggestions for reducing this burden, to Washington Headquarters Services, Directorate for Information Operations and Reports, 1215 Jefferson Davis Highway, Suite 1204, Arlington, VA 22202-4302, and to the Office of Management and Budget, Paperwork Reduction Project (0704-0188), Washington, DC 20503.

1. AGENCY USE ONLY (Leave blank)	2. REPORT DATE	3. REPORT TYPE AND DATES COVERED
	July 1997	Final Sep 92 - Sep 95

4. TITLE AND SUBTITLE

SUB-MILLIMETER WAVEGUIDE FOR MONOLITHIC CIRCUITS

6. AUTHOR(S)

Nihad I. Dib and Linda P.B. Katehi

5. FUNDING NUMBERS

C   - F19628-92-K-0027
PE - 61102F
PR - 2305
TA - C5
WU - 21

7. PERFORMING ORGANIZATION NAME(S) AND ADDRESS(ES)

University of Michigan
Radiation Laboratory, EECS Department
Ann Arbor, MI 48109-2122

8. PERFORMING ORGANIZATION REPORT NUMBER

N/A

9. SPONSORING/MONITORING AGENCY NAME(S) AND ADDRESS(ES)

Rome Laboratory/ERAC
31 Grenier Street
Hanscom AFB MA 01731-3010

10. SPONSORING/MONITORING AGENCY REPORT NUMBER

RL-TR-97-45

11. SUPPLEMENTARY NOTES

Rome Laboratory Project Engineer: A. J. Slobodnik, Jr./ERAC/(617) 337-3716

12a. DISTRIBUTION AVAILABILITY STATEMENT

Approved for public release; distribution unlimited.

12b. DISTRIBUTION CODE

13. ABSTRACT *(Maximum 200 words)*

Millimeter and sub-millimeter wave three-dimensional open dielectric structures are characterized using the Finite Difference Time Domain (FDTD) technique. The use of FDTD method allows for the accurate characterization of these components over a very wide frequency range. Three different sub-mm wave transitions to layered ridge dielectric waveguide (LRDW) are analyzed. These are found to be efficient over a wide sub-mm frequency band which makes them useful for a variety of applications. Theoretical results for a mm-wave image guide coupler show good agreement with experimental data. Sub-mm wave LRDW directional couplers are analyzed. A 3-db, 500 GHz coupler with negligible radiation loss is designed using an interative procedure. This shows that the FDTD technique can be used not only as an analysis method, but also as a design tool which takes into account all high frequency parasitic effects. A matched termination for the LRDW is described and analyzed.

14. SUBJECT TERMS

Planar Sub-Millimeter Waveguide, Layered Ridge Dielectric Waveguide, 500 GHz Directional Coupler

15. NUMBER OF PAGES

40

16. PRICE CODE

17. SECURITY CLASSIFICATION OF REPORT	18. SECURITY CLASSIFICATION OF THIS PAGE	19. SECURITY CLASSIFICATION OF ABSTRACT	20. LIMITATION OF ABSTRACT
UNCLASSIFIED	UNCLASSIFIED	UNCLASSIFIED	SAR

Contents

1 INTRODUCTION

Millimeter wave dielectric waveguides have been extensively studied during the past two decades. Examples of these waveguides include dielectric image guides [1], strip dielectric guides, insulated image guides, strip-slab guides [2], inverted strip dielectric guides [3], cladded image guides [4] and trapped image guides [5]. These waveguides are constructed from combinations of layers and ridges of various permittivities in order to provide a region wherein the propagating power is well-confined. The widths of these lines approach one guided wavelength in order to maximize field confinement. Although there are several examples of the monolithic use of these dielectric lines in the literature [6], they have been generally considered hybrid in nature.

Recently, Engel and Katehi [7] suggested the development of monolithic sub-mm guiding structures that can be realized by considering variations of the early dielectric lines. The new waveguides are made of materials which are available in monolithic technology so that they are compatible with solid-state sources (see Fig. 1). The dimensions of these monolithic guides are fractions of a guided wavelength, so the new structures may be used not only as guiding media but as means of making passive components.

The successful use of dielectric lines in a hybrid or monolithic environment relies mainly on the ability to realize an efficient transition to the dielectric waveguide. In the past, a variety of transitions from rectangular waveguide to mm-wave dielectric lines have been mainly characterized experimentally [8, 9]. When layered ridge dielectric waveguides (LRDWs) [7] are used in a monolithic environment, transitions to and out of dielectric waveguide may be realized through a short length of printed conductor line on top of the ridge (Fig. 2) [10, 11]. In this manner, the dielectric waveguide components are effectively coupled to other conventional monolithic circuit components which are printed on the same wafer. Previous work on the characterization of such a transition exclusively considered the transition operating in an ideal shielding environment which was designed
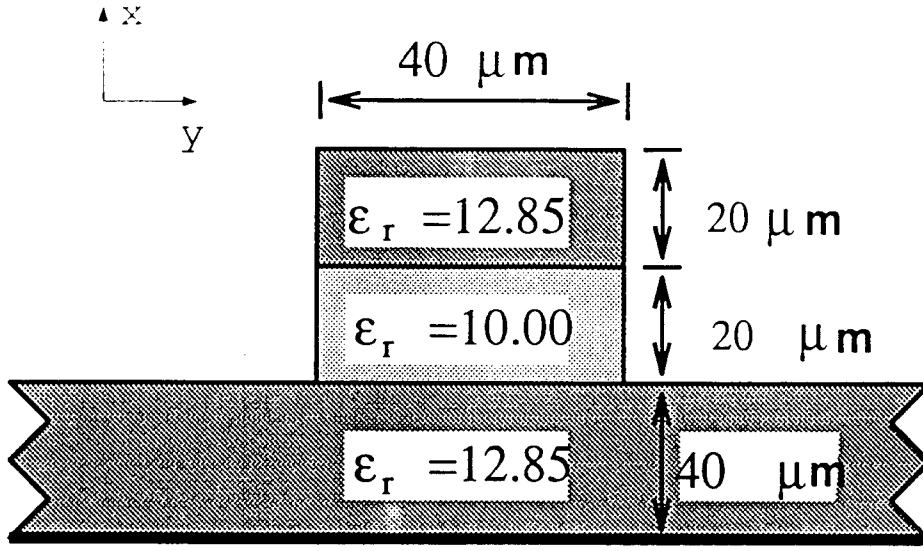
Figure 1: Cross-section of the layered ridge dielectric waveguide (LRDW) structure under study.

to effectively shield only that circuit component. As a result, the cavity was chosen adequately small enough and it was placed far enough from the transition so that it did not resonate within the frequency band and did not interfere with the circuit. The electrical performance of this ideal transition was analyzed by a hybrid full-wave integral equation-mode matching (IEMM) analysis technique and preliminary results were presented in [10]. Furthermore, a detailed study of the same shielded transition, using both the IEMM and the Finite Difference Time Domain (FDTD) methods, is presented in [11]. In practice however, monolithic circuits operate in open environments or within a larger shielding packages and may suffer from parasitic radiation (space and surface waves losses) which limits performance considerably and intensifies unwanted electromagnetic interference between circuit components. As a result, parasitic radiation needs to be studied carefully and should be accounted for during design. In this report, the above transition is studied in open environment using the FDTD technique and the effects of parasitic radiation on the transition performance are discussed. Moreover, the transition from a conventional mirostrip, printed on the substrate, to the LRDW is analyzed. The possibility of using other transitions is also discussed.
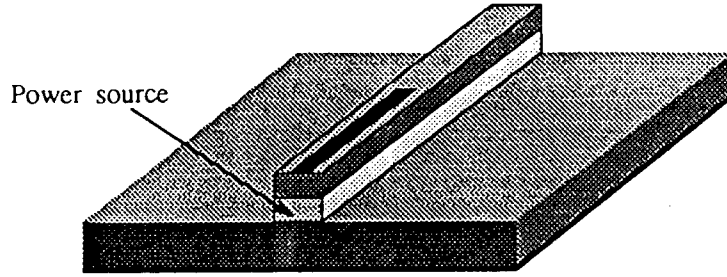
3

Figure 2: Strip-ridge line to LRDW transition. Strip width=20 μm

The second part of this work is devoted to the dielectric waveguide coupler. The distributed directional coupler, shown in Fig. 3, which consists of a section of a coupled dielectric guide of length L and separation S, presents the simplest coupler geometry. Such a coupler can be made of any type of dielectric waveguide and has been the subject of study of many publications (see for example [12]-[14]). In most of these studies the coupler design was completed by choosing the appropriate coupling length through empirical formulas for the magnitudes of S_{12} and S_{13}. This approach, however, neglects interference between the feeding lines as well as radiation loss which can be substantial in open dielectric waveguides [15] and predicts performances which are unrealizable. To overcome this problem, when comparing experimental and theoretical results, measured data had to be normalized accordingly to numerically eliminate the effect of the dielectric and radiation losses at the bends and junctions [13, 14]. In this report, the FDTD technique is used to analyze the coupler geometry and simulates the open environment in which the coupler operates by appropriate absorbing boundary conditions. For validation purposes, a mm-wave coupler which utilizes the image guide is analyzed, first, and compared to experimental data. Following this validation, a sub-mm wave directional coupler made of the LRDW shown in Fig. 1 is extensively studied. The scattering parameters and radiation loss factor of both couplers are presented.

The third part of this work concerns the issue of matching the LRDW. Looking at the field distribution on a cross section of the LRDW indicated that most of the power is confined in the
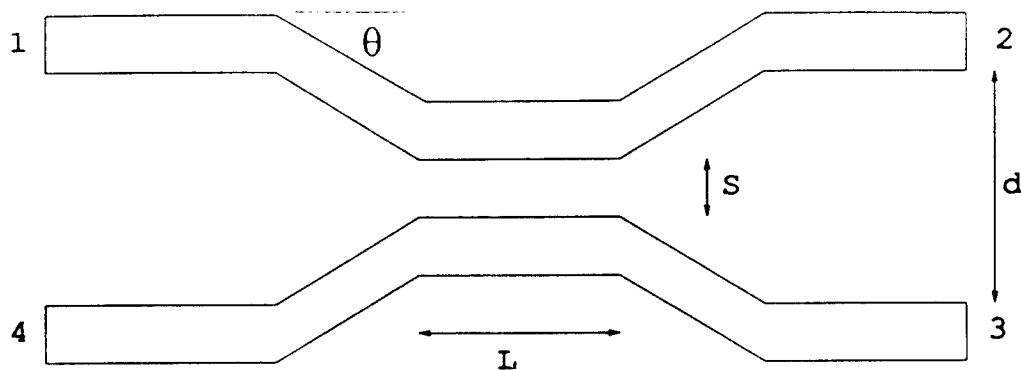
Figure 3: Top view of a distributed directional coupler.

substrate just underneath the ridge. The ridge acts only as a guiding element for the power propagating along the line. With this fact in mind, an open-end LRDW (by stopping the ridge at some point while leaving the substrate extended) is analyzed and the return loss is computed using the FDTD technique. It is shown that such an open-end may be used as a matching termination. Alternative matching terminations are also discussed.

2 THEORY

The FDTD method was first introduced by Yee [16] to solve electromagnetic scattering problems. In this method, Maxwell's curl equations are expressed in discretized space and time domains and are then used to simulate the propagation of an initial excitation in a "leapfrog" manner. Recently, the method has been successfully applied to characterize microstrip and coplanar waveguide (CPW) lines and discontinuities [17]-[24], optical integrated circuits [25, 26], and mm-wave dielectric line transitions [27]. Only a brief summary of the FDTD method is described here.

In order to characterize any planar discontinuity, propagation of a specific time-dependent function through the structure is simulated using the FDTD technique. The time dependence of the

excitation can be chosen arbitrarily. A Gaussian pulse is often used because it is smoothly varying in time and its Fourier transform is also a Gaussian function centered at zero frequency. However, since dielectric lines possess a non-zero cutoff frequency, it is more convenient to use an excitation pulse which has an amplitude spectrum in a specific frequency range. In this research, the following function is used [28]:

$$f(t) = Ce^{-\frac{(t-t_o)^2}{2T^2}} \sin(\omega t) \qquad (1)$$

$$T = \frac{\sqrt{6}}{\pi(f_{max} - f_{min})} \qquad (2)$$

$$\omega = \pi(f_{max} + f_{min}) \qquad (3)$$

$$t_0 = 3T \qquad (4)$$

where f_{min} and f_{max} are the frequencies at which the value of the spectrum is 5% of its peak which occurs at $(f_{max} + f_{min})/2$. The above function is the imaginary part of what is known as the Gabor elementary function [29]. Following the time and space discretizations of the electric and magnetic field components, the FDTD equivalents of Maxwell's equations are then used to update the spatial distributions of these components at alternating half time steps [30]. The space steps, $\triangle x$, $\triangle y$ and $\triangle z$, are carefully chosen such that integral numbers of them can approximate the various dimensions of the structure. As a rule of thumb and in order to reduce the truncation and grid dispersion errors, the maximum step size is chosen to be less than 1/20 of the smallest wavelength existing in the computational domain (i.e., at the highest frequency represented in the pulse). Then, the Courant stability criterion is used to select the time step to insure numerical stability. For the LRDW structures under study, the following parameters are used: $\triangle x$=5 μm, $\triangle y$=$\triangle z$=10 μm and $\triangle t$=0.0136 ps.

In order to excite the dielectric waveguide, the vertical electric field component at the front plane (z=0) is excited (see Fig. 4) and the magnetic wall source condition of [18] is used to compute the fields elsewhere in the plane z=0. The source distribution has been modified to take into account
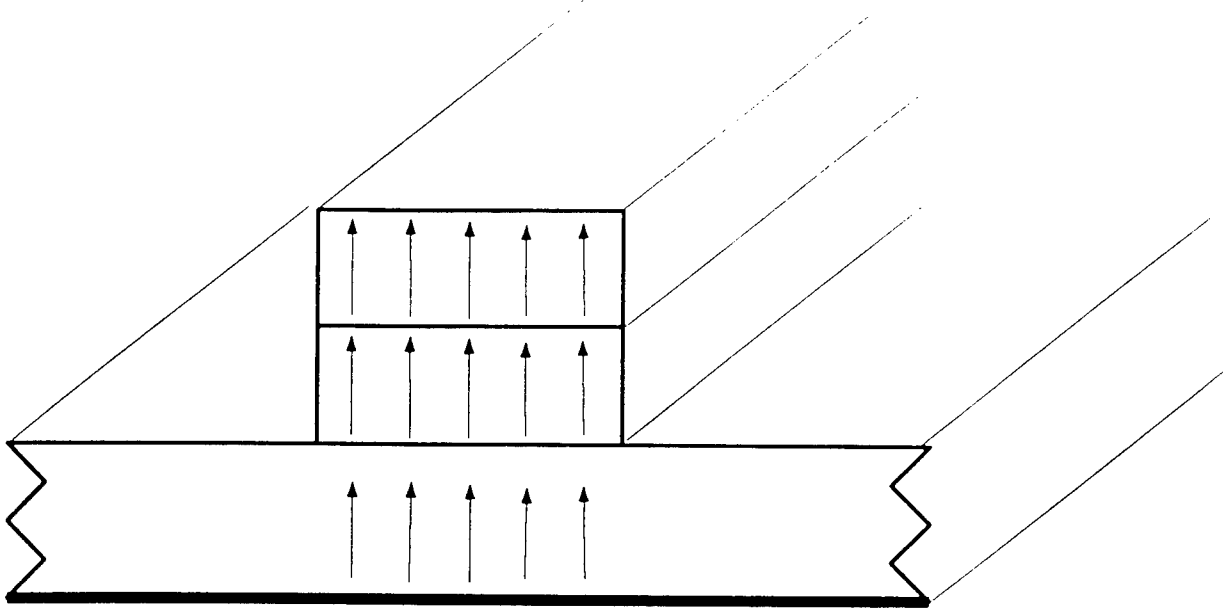
Figure 4: Excitation for the dielectric waveguide in the FDTD analysis.

the discontinuity experienced by the vertical electric field [19]. For the electric field components

lying on a dielectric-dielectric interface, the average between the two permittivities is used in the

FDTD equations [17]. The super-absorbing first-order Mur boundary condition [31, 32, 33] is

utilized to terminate the FDTD lattice at the front and back planes in order to simulate infinite

lines. This absorbing boundary condition requires a choice for the incident velocity of the waves,

or equivalently ϵ_{eff}. It has been found that an appropriate choice of $\epsilon_{r,eff}$ minimizes the effect

of the absorbing boundary walls. For the dielectric waveguide under consideration, the average

between the relative effective dielectric constants at f_{min} and f_{max} is used. These effective dielectric

constants can be obtained from the 2D-FDTD method [34, 35] or by simulating a propagating pulse

on a dielectric through line [36]. The effectiveness of these choices has been checked by performing

several numerical experiments with different values of $\epsilon_{r,eff}$. On the other hand, the first-order

Mur boundary condition is used on the top and side walls to simulate an open structure. For the

dielectric waveguide under study, the left and right absorbers were placed at a distance of 240 μm

from the edges of the dielectric line, while the top absorber was placed at a distance of 300 μm from

the top surface of the line.

In general. the frequency dependent scattering parameters. S_{ij}. can be obtained as follows [17. 18]:

$$S_{ij}(\omega) = \frac{V_i(\omega)}{V_j(\omega)} \sqrt{\frac{Z_{0j}}{Z_{0i}}} \tag{5}$$

where V_i and V_j are the voltages at ports i and j, respectively. and Z_{0j} and Z_{0i} are the wave impedances of the lines connected to these ports. In case of dielectric lines, where voltage is not uniquely defined, the vertical component of the electric field is probed and used in the above equation instead of the voltage [15]. To obtain $S_{11}(\omega)$, the incident and reflected fields must be known. Since the FDTD simulation calculates the total field which is the sum of the incident and reflected waveforms, the incident field is obtained from a line of an infinite extent and is subtracted from the total waveform to yield the reflected field.

3   RESULTS and DISCUSSION

3.1   Transitions to the LRDW

In this section, several transition structures to the LRDW are studied. Namely, strip-ridge to LRDW transition (Fig. 2), conventional microstrip to LRDW transition (Fig. 5) and rectangular waveguide to LRDW transition (Fig. 6) [37].

Before analyzing these structures, one needs to look at the dispersion diagrams of both the LRDW and the strip-ridge line. Figures 7 and 8 show the dispersion curves of the dominant propagating modes of the strip-ridge line and the LRDW, respectively. The 3D-FDTD results are obtained by simulating the propagation of a pulse through an infinite line [36]. On the other hand, the 2D-FDTD results are obtained in an implicit way where one inputs a value for the propagation constant and then finds the frequencies at which the modes propagating with this specific propagation constant can be supported [34, 35]. The 3D-FDTD has the advantage that only one simulation is needed to obtain the dispersion curve, while, the 2D-FDTD, though faster and simpler to implement, needs
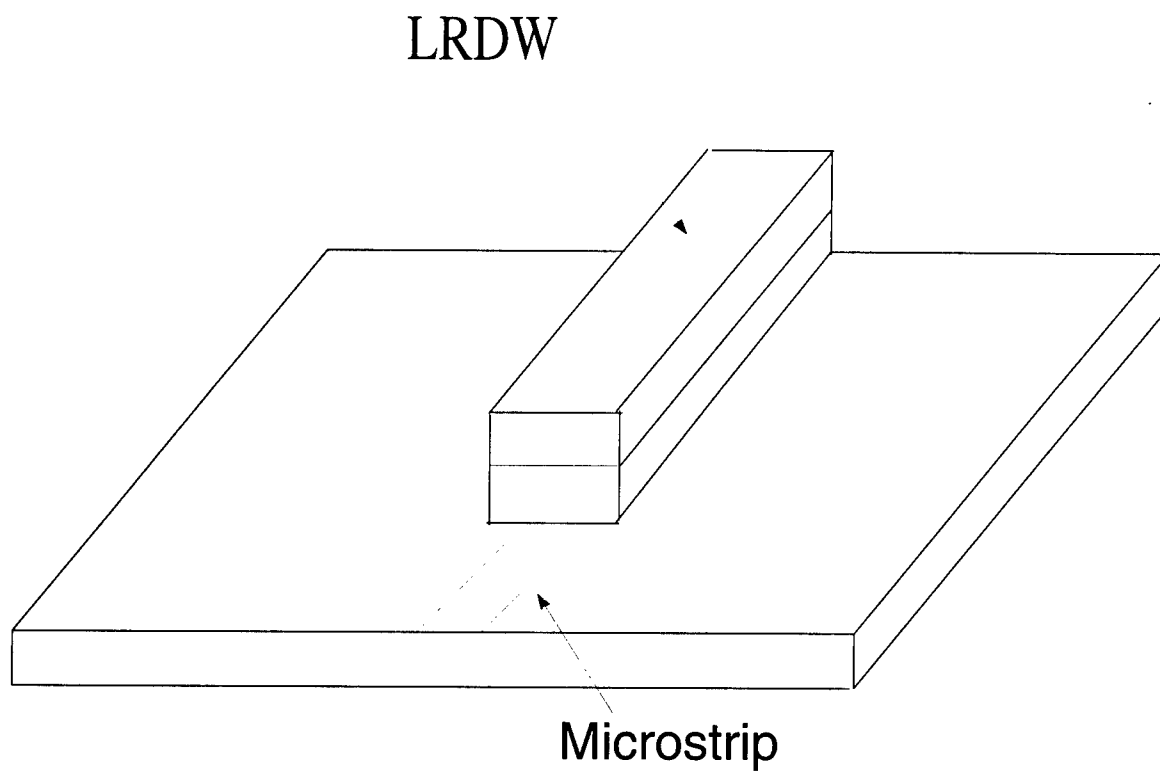
8

LRDW

Microstrip
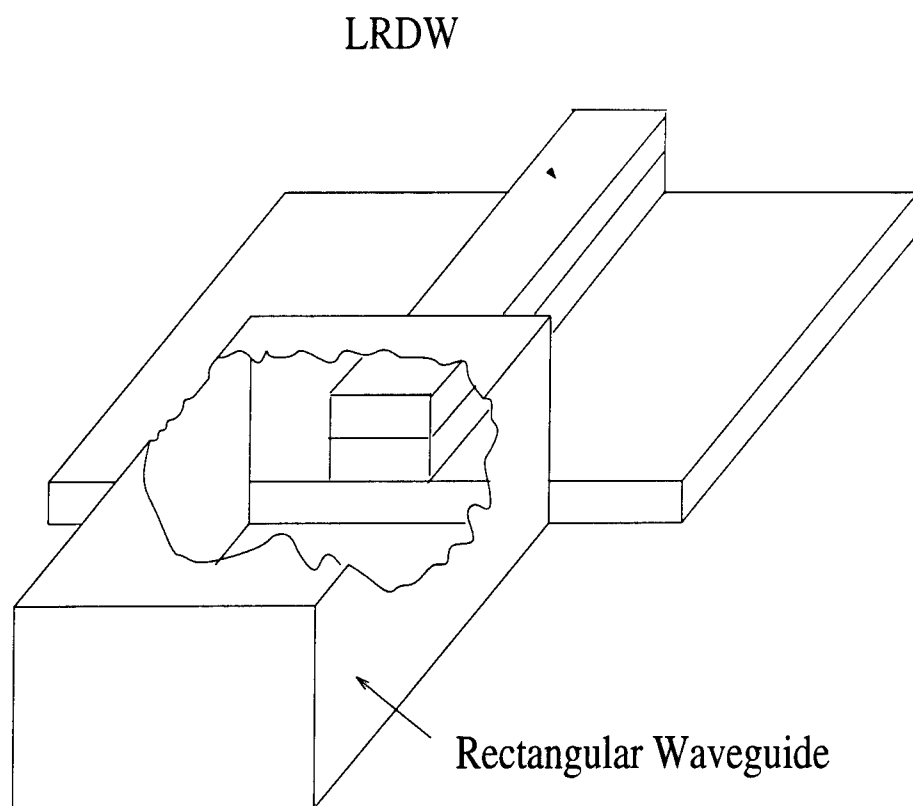
Figure 5: Microstrip to LRDW transition.
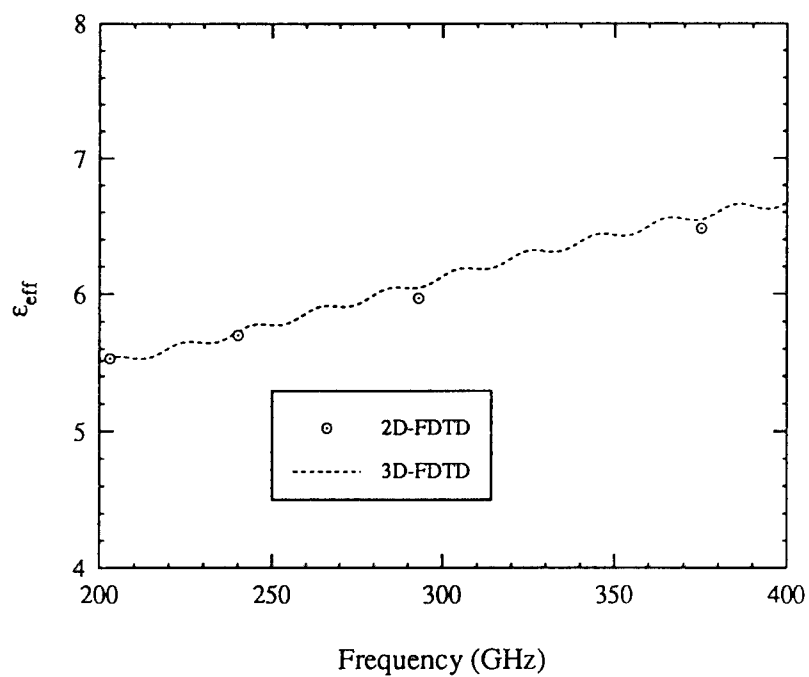
LRDW

Figure 6: Rectangular waveguide to LRDW transition.

Figure 7: Dispersion diagram for the dominant mode of the strip-ridge line with strip width of 20 μm.
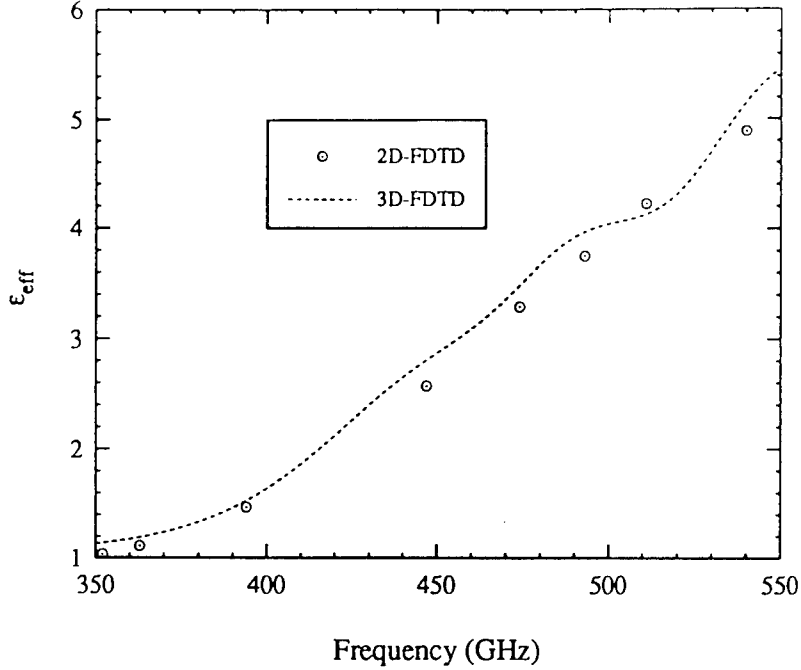
Figure 8: Dispersion diagram for the dominant mode of the layered dielectric line.

to be executed several times to give the propagation constant in a frequency range. One added

advantage of the 2D-FDTD technique, however, is its ability to predict the propagation constants

of higher order modes besides the dominant propagating mode. Figure 8 shows that the dielectric

guide dominant mode has practically a cutoff frequency around 350 GHz.

1. Strip-Ridge to LRDW Transition (Fig. 2)

Of primary interest in evaluating the performance of the the transition shown in Fig. 2 is the

power transferred from the dominant mode in the strip-ridge structure to the dominant mode

in the LRDW. Figure 9 shows the magnitude of the reflection coefficient for this transition in

the frequency range DC-550 GHz. Due to the fact that the strip-ridge to LRDW transition is

an open structure, the magnitude of S_{11} is always less than 1.0 even for frequencies below the

waveguide dominant mode cutoff frequency (around 350 GHz) while the shielded transition

showed a total reflection ($|S_{11}|=1$) in [11]. Specifically, in the open transition, for operating

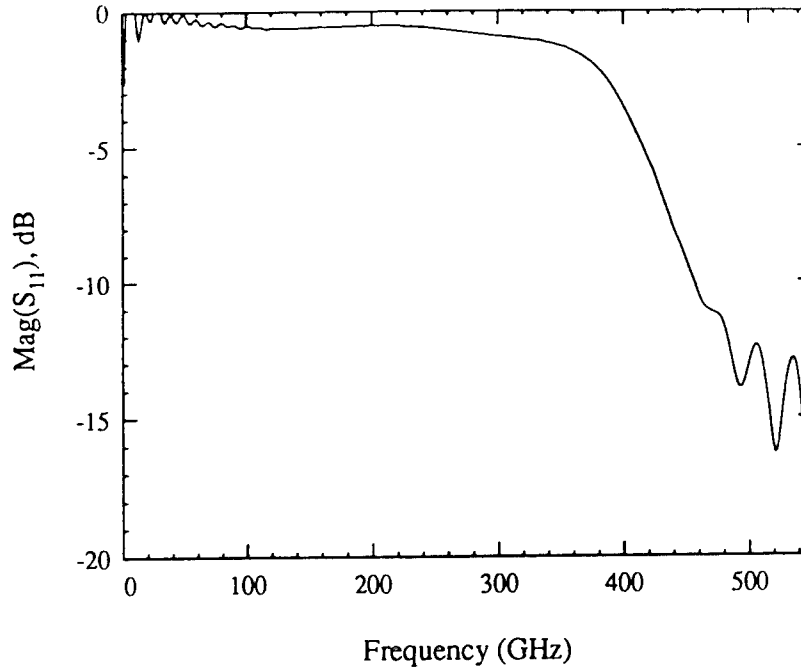frequencies between 100 and 300 GHz almost 20% of the incident power is lost in the form of

11

Figure 9: Magnitude of S_{11} for the strip-ridge to LRDW transition shown in Fig. 2.

space and surface waves which will be referred to as radiation loss in this report. However, as the operating frequency approaches 500 GHz, the return loss reduces to around -15 dB.

2. Microstrip to LRDW Transition (Fig. 5)

Figure 10 shows the magnitude of the reflection coefficient for this transition in the frequency range DC-550 GHz for different strip widths. It can be seen that the return loss for strips' widths of 40μm and 60 μm is almost the same and slightly better than that obtained with strip width of 20μm. In comparison with the strip-ridge to LRDW transition, the microstrip to LRDW transition exhibits a larger return loss. In all the above examples the dielectric waveguide ridge has a layered consistency similar to the one on Fir. 1.

3. Rectangular waveguide to LRDW transition (Fig. 6)

Figure 6 shows a transition from a recy'tangular waveguide operating in the dominant mode from 350GHz to 530GHz to a LRDW with the cross section shown on Fig. 1. Figure 11 shows
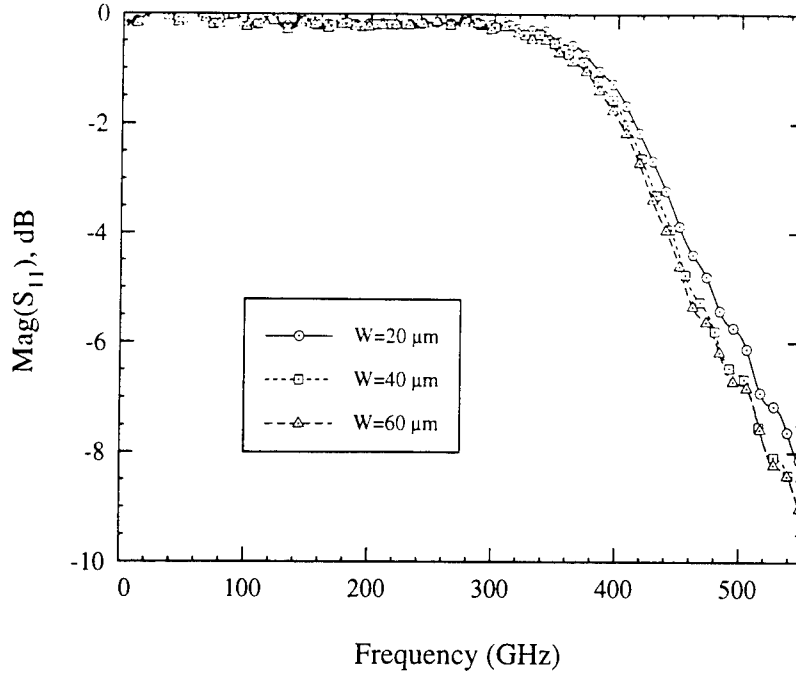
Figure 10: Magnitude of S_{11} for the conventional microstrip to LRDW transition shown in Fig. 5. W is the mirostrip width.

the magnitude of the reflection coefficient for this transition in the frequency range 350-530 GHz. It can be seen that the reflection coefficient for such a transition is less than 14 dB in the whole frequency range.

3.2 LRDW Directional Coupler

A simple design of the dielectric directional coupler is shown in Fig. 3, where θ indicates the angle between the tilted line and the horizontal axis, L is the length of the coupled LRDW sections, s is the separation between the coupled sections and d is the separation between the feeding lines. This design approach assumes zero loss, negligible coupling due to the feeding dielectric waveguides and the tapered sections and considers quasi-static interactions in the coupling region. As a result, the magnitudes of the scattering parameters S_{12} and S_{13} can be obtained from the following relations
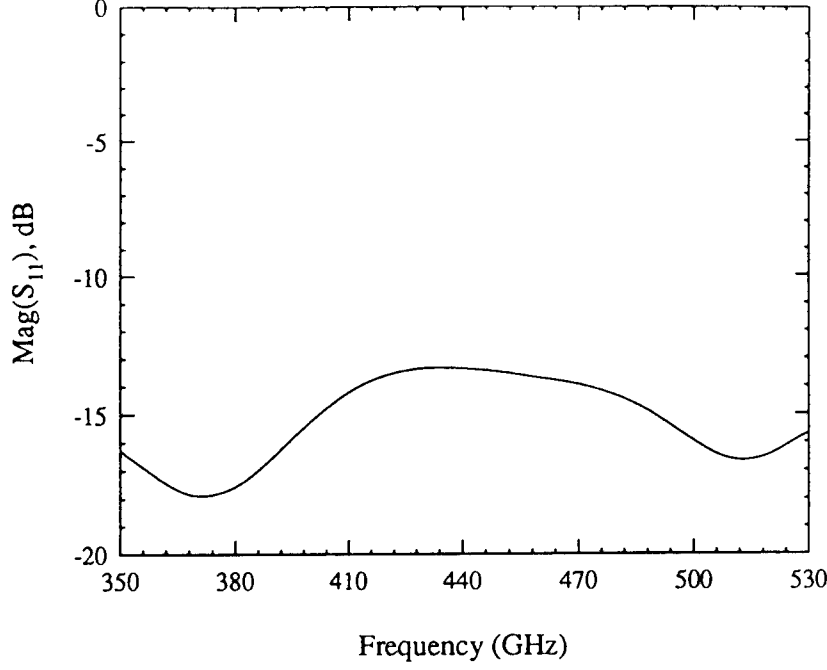
13

Figure 11: Magnitude of S_{11} for the rectangular waveguide to LRDW transition shown in Fig. 6. The waveguide has a width and height of 560μm and 280μm, respectively.

[12]-[14]:

$$| S_{12} |=| \cos\left(\frac{\beta_e - \beta_o}{2}L\right) | \tag{6}$$

$$| S_{13} |=| \sin\left(\frac{\beta_e - \beta_o}{2}L\right) | \tag{7}$$

where β_e and β_o are the even and odd propagation constants of the coupled dielectric waveguide, respectively. With the knowledge of β_e and β_o, the coupling length L can be chosen to provide a coupler with a specific coupling coefficient $|S_{13}|$. An improvement of such an ideal design can be achieved by extending the effective coupling region within the tapered sections resulting in modified equations (6) and (7) which include an effective coupling length, instead of the physical length, as suggested in [12]. The effective coupling length can be defined as:

$$L_{eff} = L + \frac{\triangle\phi}{\beta_e - \beta_o} \tag{8}$$

$$\triangle\phi = 2\int_{z_0}^{z'} [\beta_{ze}(z) - \beta_{zo}(z)]dz \tag{9}$$

14

where the integration is performed along the axial direction of the coupler. z_0 corresponds to the junction between the coupled guide and the connecting arm, while z' is chosen to be some value of z beyond which the coupling between the arms is negligible. Due to the assumed ideal conditions of operation, equations (6) and (7) cannot account for any loss in the coupler. In [38], these ideal designs have been applied to the design of several sub-millimeter-wave couplers and their predicted coupler geometries were analyzed by the FDTD technique. The predicted and numerically derived results were compared in an effort to understand the effect of radiation loss on the coupler performance. In this report, an example of a mm-wave image line coupler is investigated for validation purposes and a sub-mm wave LRDW coupler with a design frequency of 500 GHz is presented.

For validation purposes, a distributed coupler made of image dielectric line is investigated. Figure 12 shows $|S_{12}|$ and $|S_{13}|$ of the image guide coupler compared to the experimental results from [39]. Considering the fact that the experimental results were obtained through an implicit measurement with the assumption that the coupler is lossless, qualitative agreement between theory and experiment is satisfactory. The magnitude of S_{11} is found to be less than -30 dB in the whole frequency range which agrees with the experimental results in [39]. Figure 13 shows the amount of radiated power from such a coupler which further verifies that radiation losses can not be neglected. It is worth mentioning that the FDTD obtained frequency at which $|S_{12}|$ and $|S_{13}|$ intersect agrees very well with that obtained using equations (6) and (7) in conjunction with (8) and (9) (see Figure 13 in [39]). It should be mentioned that the tapered sections of the dielectric guide are modeled using the "staircase" approximation.

Using (6) and (7) in conjunction with the propagation constants of the even and odd modes (obtained using 2D-FDTD), it was found that a coupling length L of approximately 200μm should give a 3dB coupler with a design frequency of 500 GHz. The separation between the two LRDWs in the coupler is 40 μm. Figure 14 shows the scattering parameters of this coupler with a coupling
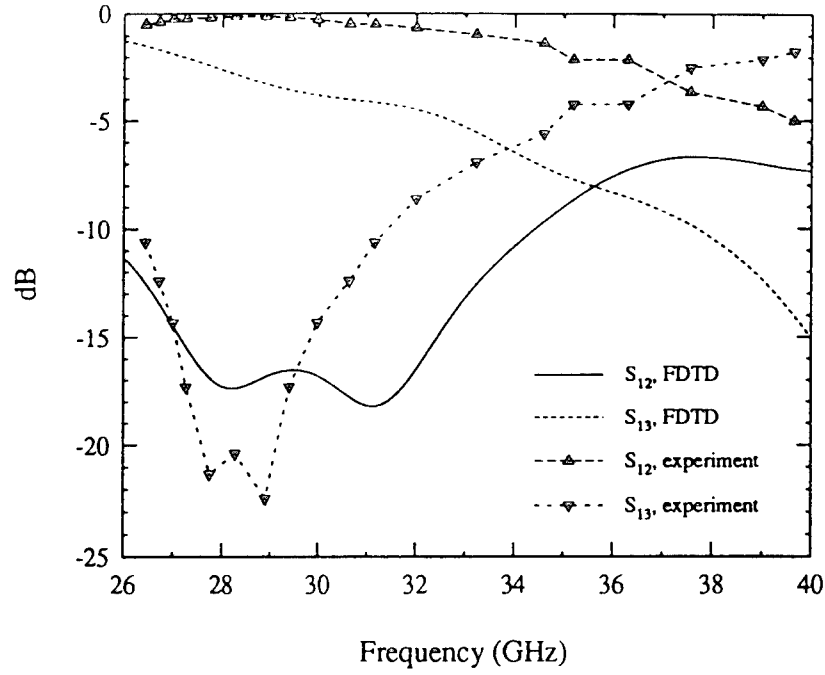
15

Figure 12: Magnitudes of S_{12} and S_{13} of the image guide coupler compared to the experimental results from [39]. S= 2.4 mm, image guide width= 4.8 mm, image guide height= 2.4 mm, ϵ_r= 2.22, L=59 mm, θ=26°, and d=9.6 mm.
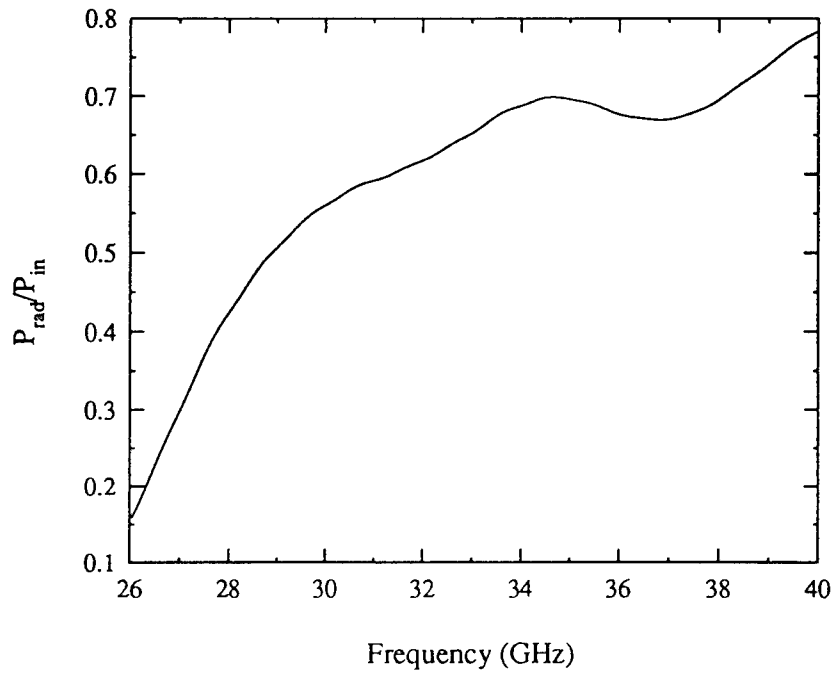

Figure 13: Radiation loss factor $(1 - |S_{11}|^2 - |S_{12}|^2 - |S_{13}|^2 - |S_{14}^2)$ of the image guide coupler.

length of 250μm. The sources of the discrepancy between these simulated results and the ideal response. which should have a 3dB design frequency around 500 GHz. are the effects of the junctions and the coupling between the connecting guides. Moreover. Fig. 14 shows radiation loss as predicted by the FDTD method. From this figure. it can be seen that at 490 GHz. almost 15% of the input power is lost as parasitic radiation in the form of space and surface waves.

Figure 15 shows the results for the same coupler with a coupling length L of 300μm. In this case. S_{12} and S_{13} intersect at 488 GHz with a value of -3.8 dB. With this in mind, the coupling length L was increased to 330μm in order to get a design frequency closer to 500 GHz. Figure 16 shows the results for the coupler. In this case, S_{12} and S_{13} intersect at approximately 500 GHz with a value of -4 dB. Finally, a coupler with GaAs used in the middle layer (i.e., ϵ_r=12.85 instead of 10) was analyzed and its response was found to be similar to that shown in Fig. 16 except that the values of S_{12} and S_{13} at the design frequency (500 GHz) were -5 dB and the radiation loss was somewhat higher than that shown in Fig. 16.

3.3 Matched Termination

Using the 2D-FDTD method, it was found that in the LRDW shown in Fig. 1, most of the power is confined in the substrate just underneath the ridge. The ridge acts only as a guiding element for the power propagating along the line. With this fact in mind, we analyzed an open-end LRDW (by stopping the ridge at some point while leaving the substrate extended). The return loss of such an open-end is shown in Fig. 17. A return loss of less than 16 dB in the frequency range 450 to 550 GHz is obtained. Thus, such an open-end may be used as a matching termination to the LRDW.

Figure 18 shows the scattering parameters of an LRDW coupler with port 4 open-ended. It can be seen that S_{12} and S_{13} intersect at 505 GHz with value of -3.8 dB.

Other matching mechanisms can be used. For example, a lossy material that absorbs power at sub-millimeter waves situated at the end of the LRDW can act as a matched termination.
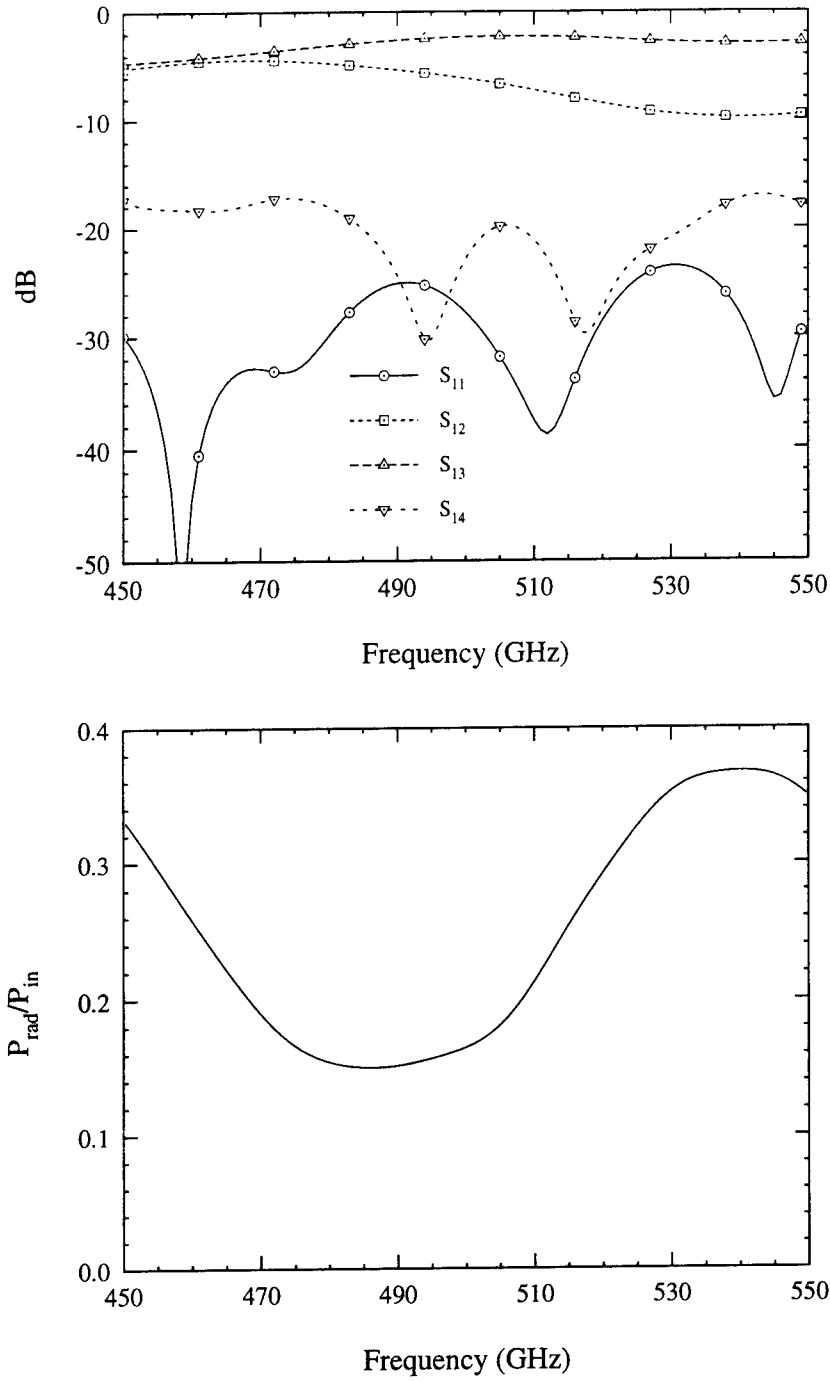
Figure 14: Scattering parameters and Radiation loss factor of the LRDW coupler obtained using the FDTD technique.

S=40 μm, L=250 μm, d=320 μm, θ= 26°.

Figure 15: Scattering parameters and Radiation loss factor of the LRDW coupler obtained using the FDTD technique.

S=40 μm, L=300 μm, d=320 μm, θ= 26°.
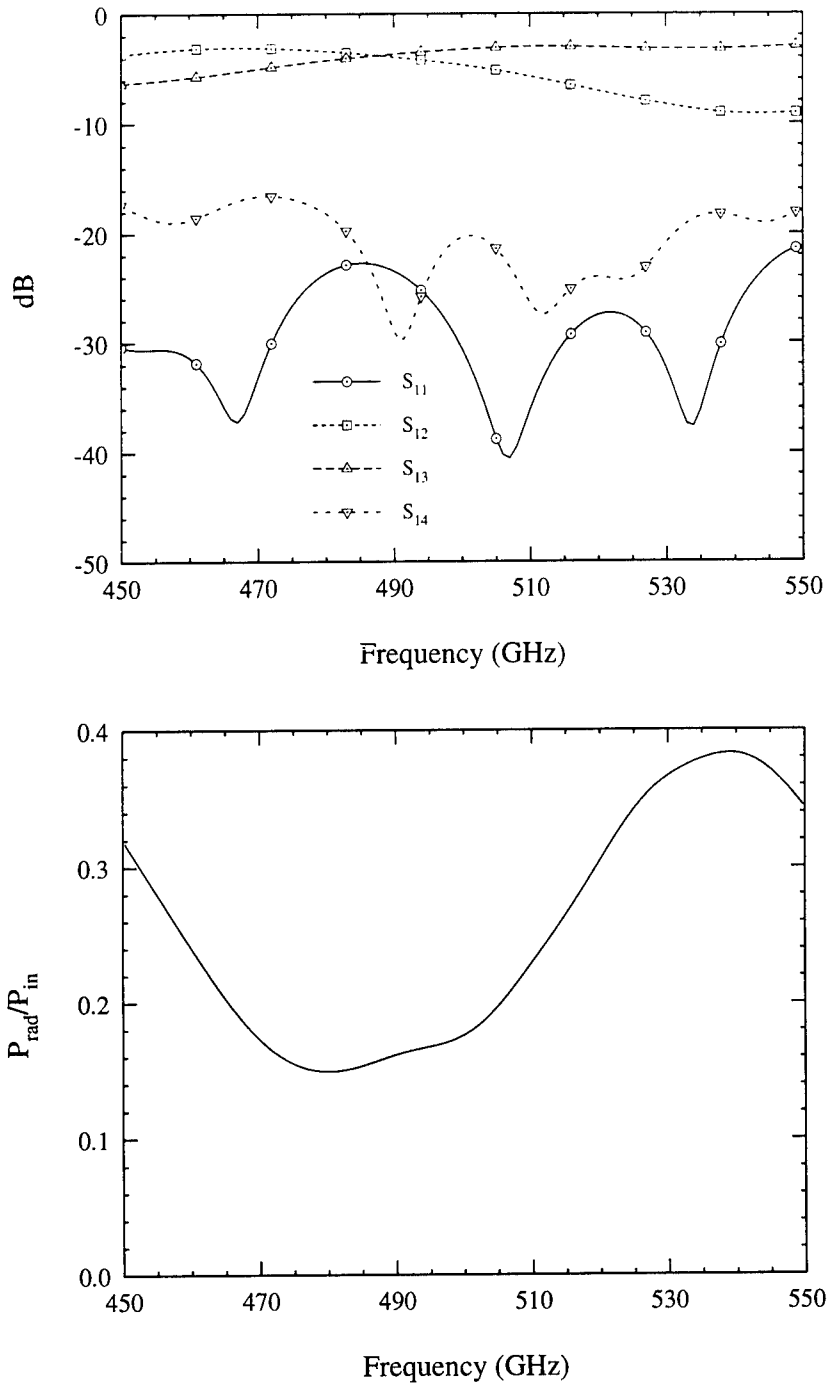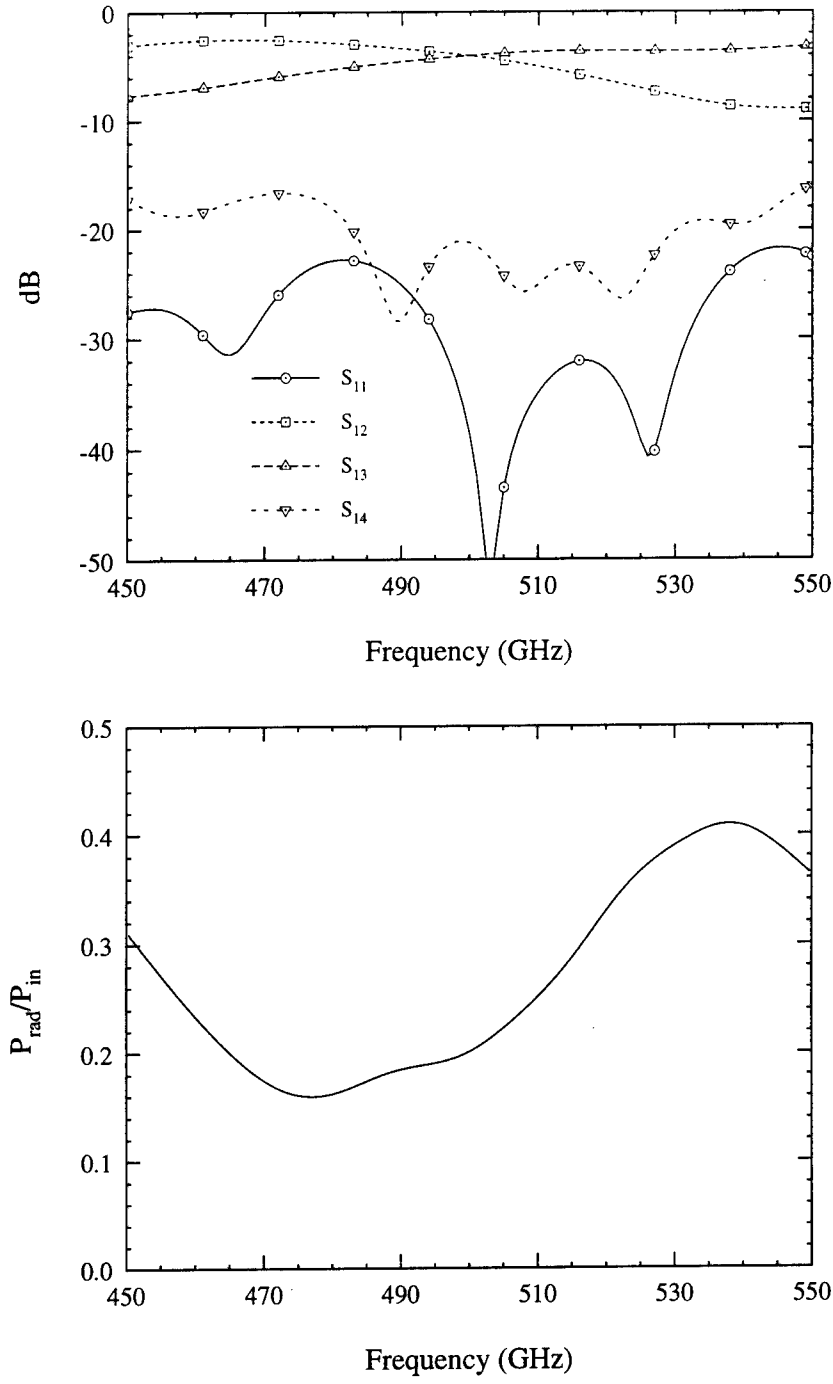
Figure 16: Scattering parameters and Radiation loss factor of the LRDW coupler obtained using the FDTD technique.
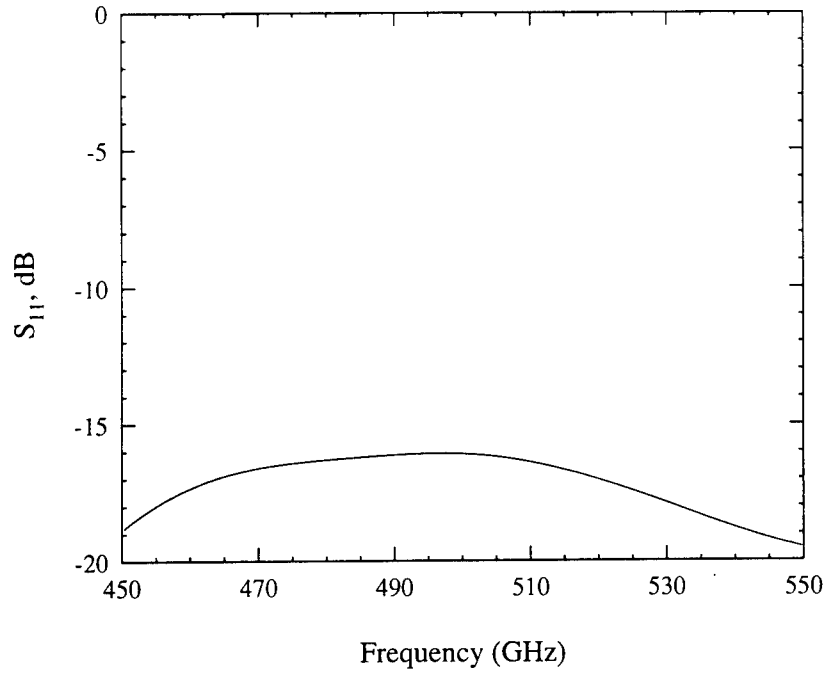
S=40 μm, L=330 μm, d=320 μm, θ= 26°.
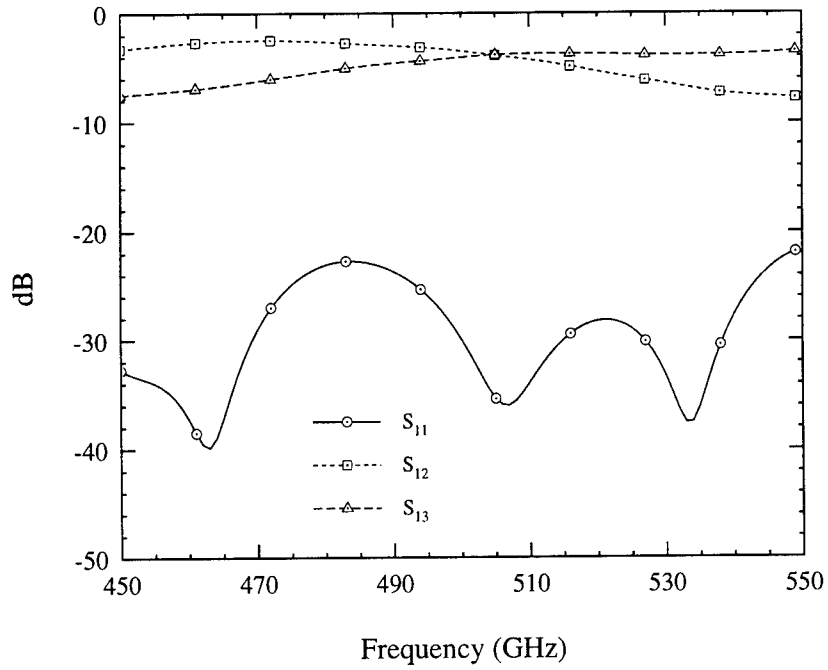
Figure 17: Return loss of an open-end LRDW.

Figure 18: Scattering parameters of the LRDW coupler with port 4 open-ended. S=40 μm, L=300 μm, d=320 μm, θ= 26°.

Alternatively. the LRDW may be transitioned to a rectangular waveguide which is then terminated properly.

4 Design Guidelines

In the design of the above coupler, the following steps have been followed:

1. The thicknesses and the relative permittivities of the layers are specified.

2. The 2D-FDTD method is used to obtain the dispersion diagram of the single LRDW under consideration. This is done in order to know the value of the effective dielectric constant to be used at the front and back absorbers when the 3D-FDTD method is executed to analyze the coupler.

3. The separation distance between the two coupled LRDWs, to be used in the coupler, is specified.

4. The 2D-FDTD method is used to obtain the even and odd propagation constants of the coupled LRDWs structure in a specific frequency range. From these propagation constants, equations (6) and (7) are used to determine the coupling length needed to achieve a specific coupling ratio at the design frequency.

5. The 3D-FDTD method is used to analyze the coupler with the above specifications. Most likely, the results will not be as expected because of the parasitic radiation effects. Thus, the 3D-FDTD method is executed for different coupling lengths until the desired characteristics are obtained.

5 Description of FDTD Methods

5.1 2D-FDTD

The 2D-FDTD method is based on the technique presented in [34, 40, 41]. In this technique, the 3D standard Yee's cell [16] is reduced to a 2D cell. This technique can be used to obtain the dispersion diagram of any waveguide structure or transmission line. Thus, instead of discretizing a 3D mesh, only the cross section of the line under consideration is discretized.

Note that in obtaining the dispersion diagram of the single LRDW shown in Fig. 1, only one sample point is included that corresponds to β=21000 rad/sec. It should be emphasized that in 2D-FDTD, the propagation constant β is chosen first and then the frequencies, at which there exist modes propagating with this specific β, are obtained. This is in contrast to frequency domain techniques in which the opposite usually happens. The space steps, $\triangle x$ and $\triangle y$ are carefully chosen such that integral numbers of them can approximate the various dimensions of the structure. As a rule of thumb and in order to reduce the truncation and grid dispersion errors, the maximum step size is chosen to be less than 1/20 of the smallest wavelength occurring at the highest frequency of interest. Then, the Courant stability criterion is used to select the time step to insure numerical stability. For the LRDW under study, the following parameters are used: $\triangle x$=5.0 μm, $\triangle y$=10 μm and $\triangle t$=0.01489 ps. The number of time steps (ts) is chosen large enough (e.g., 10000) to let the fields reach the steady state. One might experiment with this parameter to check the convergence of the final result. In order to excite the computational domain, several impulses are assumed to exist at arbitrary nodes. This will give all modes that can be supported by the guide. However, one may change the program such that a specific initial condition with a specific kind of symmetry is assumed. It is also necessary to specify the number of different regions that the computational domain is composed of. Then, the relative permittivities of all regions have to be entered (notice that anisotropic materials are assumed). Finally, the location of any horizontal or vertical perfectly
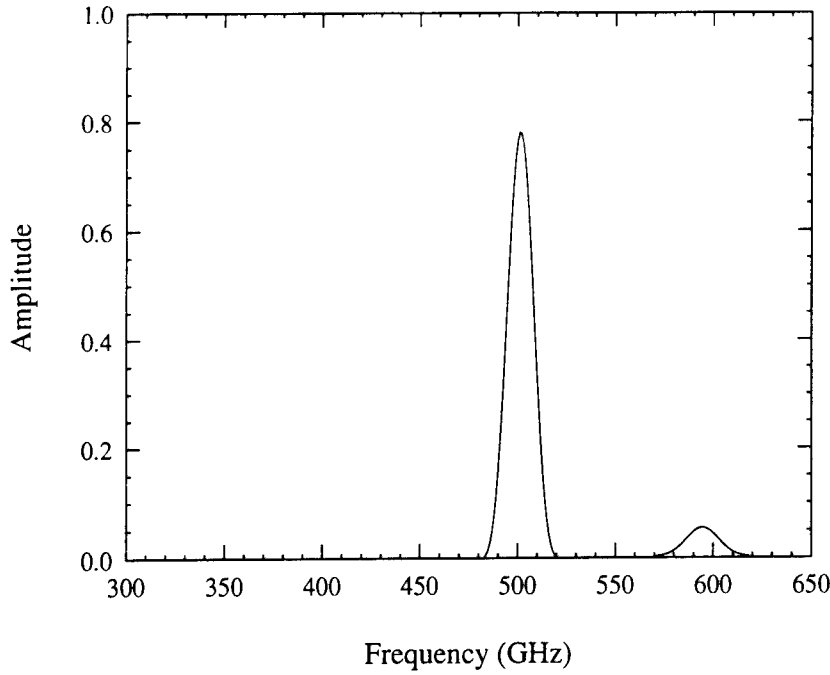
Figure 19: Example of Fourier Transform Results

electric conductors (PECs), other than the ground plane, have to be specified. Clearly, there are no PECs for the case of the LRDW. Once the FDTD time loop is done, data is created which contains the value of the probed field component as a function of time step. Then, the frequency range in which the discrete Fourier transform of the probed field is required is requested. The results of this Fourier transform contain the amplitude as a function of frequency. Fig. 19 shows a plot of a typical example. The two peaks seen in the figure correspond to the propagating modes that can be supported by the LRDW with the appriori chosen β. The first peak corresponds to the dominant mode while the second one corresponds to the first higher order mode. Finally, choosing other values of β and obtaining the corresponding frequencies gives the dispersion diagram shown in Fig. 8.

Similarly, one can obtain the dispersion characteristics of the even and odd modes of the coupled LRDWs. However, in this case, one needs to enforce the symmetry to be able to tell which mode corresponds to the odd mode and which one corresponds to the even mode. A somewhat modified

24

2D-FDTD method is used in the case of coupled dielectrics to obtain propagation. These propagation constants will be used later in conjunction with equations 6 and 7 to obtain an estimate of the desired coupling length. It should be emphasized that in the case of coupled dielectrics, a specific initial field distribution is used to enforce the even or odd symmetry.

5.2   3D-FDTD

The 3D-FDTD method is based on the conventional Yee's FDTD scheme [16]. It is necessary to run an LRDW through line before analyzing the coupler in order to obtain the incident pulse waveform which is used later to derive the scattering parameters as was discussed in the theory section. It should be noted that the definition of the regions here is similar to that applicable above except for the fact that the regions are three dimensional in this case instead of being two dimensional. Figure 20 shows the field component E_x at some distance along the line as a function of time step. Some reflections can be noticed due to the imperfections in the absorber at the back wall of the computational domain. This is due to the fact that a wide band pulse (350-600 GHz) was used as an excitation. Figure 21 shows E_x as a function of time for a narrower band pulse that extends from 450-550 GHz. In this case, an ϵ_{eff} of 4.0 is used at the front and back walls. It can be noticed that the reflections from the absorber have diminished to a negligible value.

When a through line is analyzed, one can easily get the effective dielectric constant of the line as a function of frequency using transmission line theory [18]. Two probes at a distance of $10\triangle z$ are usually used to derive the propagation constant.

For the analysis of the LRDW coupler (see for example Fig. 18) the tapered sections have to be discretized properly using the "staircase" approximation. The field component E_x is probed in 4 locations, each at a different port. The scattering parameters S_{11}, S_{12}, S_{13} and S_{14} can then be calulated.
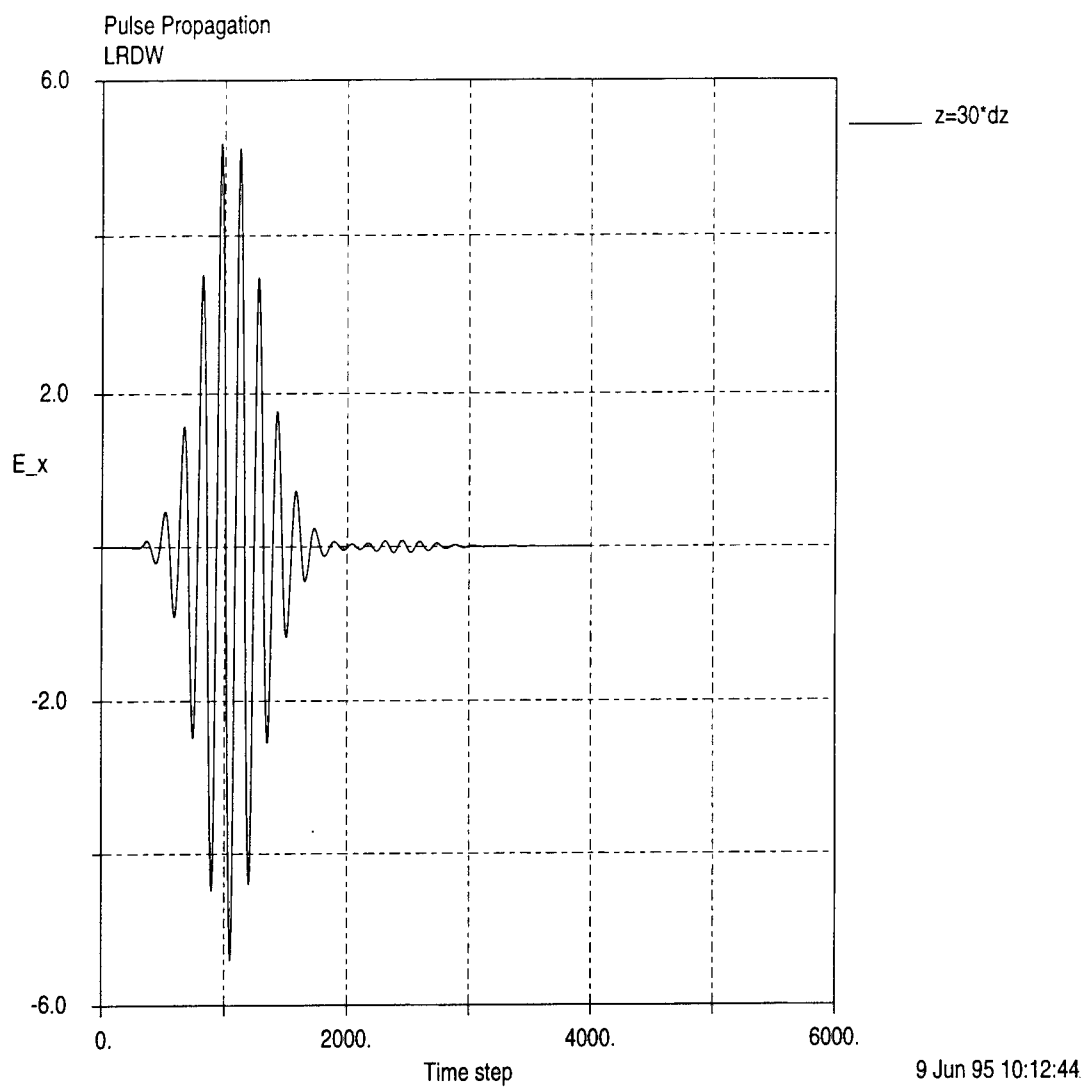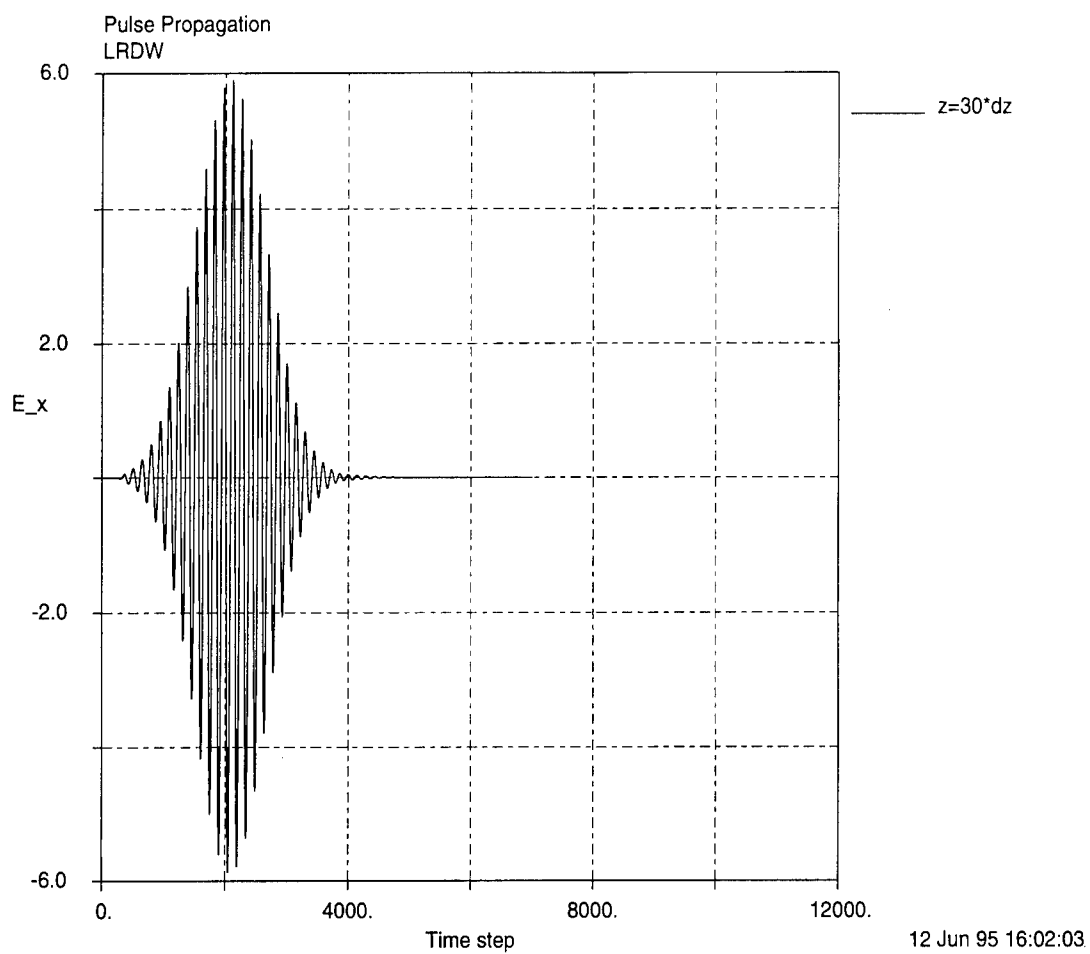
Figure 20: A plot of the field component E_x.

Figure 21: A plot of the field components E_x

References

[1] K. Solbach and I. Wolff. "The Electromagnetic Fields and the Phase Constants of Dielectric Image Lines," *IEEE Trans. Microwave Theory and Techniques.* pp. 266-274. Apr. 1978.

[2] W. McLevige, T. Itoh and R. Mittra. "New Waveguide Structures for Millimeter-Wave and Optical Circuits," *IEEE Trans. Microwave Theory and Techniques,* pp. 788-794, Oct. 1975.

[3] T. Itoh, "Inverted Strip Dielectric Waveguide for Millimeter Wave Integrated Circuits," *IEEE Trans. Microwave Theory and Techniques,* pp. 821-827, Nov. 1976.

[4] K. Ogusu, "Numerical Analysis of the Rectangular Dielectric Waveguide and its Modifications, " *IEEE Trans. Microwave Theory and Techniques,* pp. 875-885, Nov. 1977.

[5] T. Itoh and B. Adelseck, "Trapped Image Guide for Millimeter-Wave Circuits, *IEEE Trans. Microwave Theory and Techniques,* pp. 1433-1436, Dec. 1980.

[6] T. Wang and S. Schwarz, "Design of Dielectric Ridge Waveguides for Millimeter Wave Integrated Circuits, " *IEEE Trans. Microwave Theory and Techniques* , pp. 128-134, Feb. 1983.

[7] A. G. Engel, Jr. and P. B. Katehi, "Low-loss monolithic transmission lines for sub-millimeter and terahertz frequency applications," *IEEE Trans. Microwave Theory and Techniques,* pp. 1847–1854, Nov. 1991.

[8] J. Malherbe, J. Cloete and I. Losch, "A Transition from Rectangular to Nonradiating Dielectric Waveguide, " *IEEE Trans. Microwave Theory and Techniques,* pp. 539-543, June 1985.

[9] S. Bhooshan and R. Mittra, "On the Design of Transitions Between a Metal and Inverted Strip Dielectric Waveguide for Millimeter Waves, " *IEEE Trans. Microwave Theory and Techniques,* pp. 263-265, March 1981.

[10] A. G. Engel. Jr.. and L. P. B. Katehi. "On the analysis of a transition to a layered ridged dielectric waveguide." *1992 IEEE MTT-S Intl. Microwave Symp. Dig.*, pp. 983-986.

[11] A. Engel. N. Dib and L. Katehi. "Characterization of a Shielded Transition to a Dielectric Waveguide, " *IEEE Trans. Microwave Theory and Techniques*. pp. 847-854, May 1994.

[12] R. Rudokas and T. Itoh, "Passive Millimeter-Wave IC Components Made of Inverted Strip Dielectric Waveguides, " *IEEE Trans. Microwave Theory and Techniques*, pp. 978-981, Dec. 1976.

[13] J. Miao and T. Itoh, "Hollow Image Guide and Overlayed Image Guide Coupler, " *IEEE Trans. Microwave Theory and Techniques*, pp. 1826-1831, Nov. 1982.

[14] J. Rodriguez and A. Prieto, "Wide-Band Directional Couplers in Dielectric Waveguide, " *IEEE Trans. Microwave Theory and Techniques*, pp. 681-686, Aug. 1987.

[15] K. Solbach, "Electric Probe Measurements on Dielectric Image Lines in the Frequency Range of 26-90 GHz, " *IEEE Trans. Microwave Theory and Techniques*, pp. 755-758, Oct. 1978.

[16] K. S. Yee, "Numerical solution of initial boundary value problems involving Maxwell's equations in isotropic media," *IEEE Trans. Antennas Propagation* , pp. 302-307, May 1966.

[17] X. Zhang and K. Mei, "Time-domain finite difference approach to the calculation of the frequency-dependent characteristics of microstrip discontinuities, " *IEEE Trans. Microwave Theory and Techniques*, pp. 1775–1787, Dec. 1988.

[18] D. Sheen, S. Ali, M. Abouzahra and J. Kong, "Application of the Three-Dimensional Finite-Difference Time-Domain Method to the Analysis of Planar Microstrip Circuits, " *IEEE Trans. Microwave Theory and Techniques*, pp. 849–857, July 1990.

[19] L. Wu and H. Chang. "Analysis of dispersion and series gap discontinuity in shielded suspended striplines with substrate mounting grooves." *IEEE Trans. Microwave Theory and Techniques*, pp. 279–284, Feb. 1992.

[20] G. Liang, Y. Liu and K. Mei. "Full-wave Analysis of Coplanar Waveguide and Slotline Using the Time-Domain Finite-Difference Method," *IEEE Trans. Microwave Theory Tech.*, pp. 1949,1957, Dec. 1989.

[21] I. Wolff, "Finite Difference Time-Domain Simulation of Electromagnetic Fields and Microwave Circuits," *Int. J. of Numerical Modeling : Electronic Networks, Devices and Fields*, Vol. 5, pp. 163-182, 1992.

[22] W. Ko, "Time Domain Solution of Electromagnetic Problems," *Electromagnetics*, Vol. 12, pp. 403-433, 1992.

[23] T. Shibata and H. Kimura, "Computer-Aided Engineering for Microwave and Millimeter-Wave Circuits Using the FD-TD Technique of Field Simulations," *It. J. of Microwave and Millimeter-Wave Computer-Aided Engineering*, Vol. 3, No. 3, pp. 238-250, 1993.

[24] S. Visan, O. Picon and V. Hanna, "3D Characterization of Air Bridges and Via Holes in Conductor-Backed Coplanar Waveguides for MMIC Applications," *1993 IEEE MTT-S Intl. Microwave Symp. Dig.*, pp. 709-712.

[25] S. Chu, W. Huang and S. Chaudhuri, "Simulation and Analysis of Waveguide Based Optical Integrated Circuits," *Computer Physics Communications*, vol. 68, pp. 451-484, 1991.

[26] S. Chu, S. Chaudhuri and W. Huang, "Analysis of Optical Guided-Wave Devices with the FDTD Method," *1992 IEEE AP-S Intl. Symp. Digest*, pp. 257-260.

[27] N. Dib and L. Katehi, "Analysis of the Transition from Rectangular Waveguide to Shielded Dielectric Image Guide Using the Finite-Difference Time-Domain Method," *IEEE Microwave and Guided Wave Letters*, pp. 327-329, Sep. 1993.

[28] F. Moglie, T. Rozzi and P. Marcozzi, "Circuit Modeling of Waveguide Discontinuities by FD-TD methods," *Proc. of 1993 European Microwave conference*, pp. 668-669.

[29] D. Gabor, "Theory of Communication," *J. Inst. Elec. Eng.*, Vol. 93, pp. 429-457, Nov. 1946.

[30] K. Kunz and R. Luebbers, *The Finite Difference Time Domain Method for Electromagnetics*, Florida: CRC press, 1993.

[31] G. Mur, "Absorbing boundary conditions for the finite-difference approximation of the time-domain electromagnetic-field equations," *IEEE Trans. Electromagnetic Compatibility*, pp. 377–382, Nov. 1981.

[32] K. Mei and J. Fang, "Superabsorbtion-A method to improve absorbing boundary conditions," *IEEE Trans. Antennas Propagation*, pp. 1001–1010, Sep. 1992.

[33] V. Betz and R. Mittra, "Comparison and Evaluation of Boundary Conditions for the Absorption of Guided Waves in an FDTD Simulation," *IEEE Microwave and Guided Wave Letters*, pp. 499–501, Dec. 1992.

[34] A. Asi and L. Shafai, " Dispersion Analysis of Anisotropic Inhomogeneous Waveguides Using Compact 2D-FDTD," *Electronics Letters*, pp. 1451-1452, July 1992.

[35] N. Dib and L. Katehi, "Dispersion Analysis of Multilayer Planar Lines Containing Ferrite Regions Using an Extended 2D-FDTD Method," *1993 IEEE AP-S International Symposium Digest*, pp. 842-845.

[36] X. Zhang, J. Fang, K. Mei and Y. Liu, "Calculation of the dispersive characteristics of microstrips by the time-domain finite difference method," *IEEE Trans. Microwave Theory and Techniques,* pp. 263–267, Feb. 1988.

[37] G. Ponchak, N. Dib and L. Katehi, "A Novel Transition Between Rectangular Waveguide and Layered Ridge Dielectric Waveguide," Proc. of the *1994 European Microwave Conference,* pp. 1933-1937.

[38] N. Dib and L. Katehi, "Characterization of Three-Dimensional Open Dielectric Structures Using the Finite Difference Time Domain Method," submitted to the IEEE Trans. on Microwave Theory and Techniques.

[39] K. Solbach, "The Calculation and Measurement of the Coupling Properties of Dielectric Image Lines of Rectangular Cross Section," *IEEE Trans. Microwave Theory and Techniques,* pp. 54-58, Jan. 1979.

[40] G. Zheng and K. Chen, " Effects of Substrate Anisotropy on the Dispersion of Transient Signals in Microstrip Lines," *Int. J. of Infrared and Millimeter Waves,* pp. 489-498, April 1990.

[41] F. Arndt, V. Brankovic and D. Krupezevic, " An Improved FD-TD Full Wave Analysis for Arbitrary Guiding Structures Using a Two-Dimensional Mesh," 1992 IEEE MTT-S Digest, pp. 389-392.

MISSION
OF
ROME LABORATORY

Mission. The mission of Rome Laboratory is to advance the science and technologies of command, control, communications and intelligence and to transition them into systems to meet customer needs. To achieve this, Rome Lab:

    a. Conducts vigorous research, development and test programs in all applicable technologies;

    b. Transitions technology to current and future systems to improve operational capability, readiness, and supportability;

    c. Provides a full range of technical support to Air Force Material Command product centers and other Air Force organizations;

    d. Promotes transfer of technology to the private sector;

    e. Maintains leading edge technological expertise in the areas of surveillance, communications, command and control, intelligence, reliability science, electro-magnetic technology, photonics, signal processing, and computational science.

The thrust areas of technical competence include: Surveillance, Communications, Command and Control, Intelligence, Signal Processing, Computer Science and Technology, Electromagnetic Technology, Photonics and Reliability Sciences.